Scientific Research and Essays Vol. 5(3), pp. 260-274, 4 February, 2010
Available online at http://www.academicjournals.org/SRE
ISSN 1992-2248 © 2010 Academic Journals

Full Length Research Paper

Determination of geometric deformations in image registration using geometric and radiometric measurements

Fevzi Karsli* and Mustafa Dihkan

Department of Geomatics, Engineering Faculty, Karadeniz Technical University, 61080 Trabzon, Turkey.

Accepted 12 January, 2010

This paper presents a unified method based on pixels for identifying the geometric deformations of digital images. This method uses radiometric pixel gray values to represent the geometric deformations over the entire image surface, a test plate with a 38 × 22 grid, along x and y directions. This method uses a test plate to measure the radiometric pixel gray values in images which represent the geometric deformations in the image. For image registration and the detection of the geometric deformations the following six geometric transformation methods were utilized; non-reflective similarity, similarity, affine, projective, polynomial, piecewise linear and three resampling methods; nearest neighbour, bilinear and bicubic were used. The image data were taken by using Olympus E-150 digital SLR camera and the applied geometric transformation and resampling methods were coded in Matlab software. The experimental results of all the methods are presented and evaluated. The results showed that non-reflective similarity, similarity and affine transformations have a better accuracy than the other methods. Furthermore, geometric distortions were calculated by using corresponding grid corners of pixel coordinates in normal and registered images. Among all geometric transformation, projective transformation combined with three resampling methods revealed the best results.

Key words: Digital image, transformation, geometric deformations, registration, resampling.

INTRODUCTION

Image registration is the process of overlaying two or more images of the same scene taken at different times, from different viewpoints and/or by different sensors, or the process between points and one image covering the same area. It is the process of spatially aligning two or more images of a scene, consequently determining point by point correspondence between the images (Goshtasby, 1988; Brown, 1992). Image registration is a crucial stage in all image analysis tasks in which the final information is gained from the combination of various data sources such as image fusion, change detection, orthorectification and multichannel image restoration. Typically, registration is required in remote sensing (multispectral classification, environmental monitoring, change detection, creating image mosaic, weather forecasting, creating super-resolution images, integrating information into geographic information systems), medicine, cartography (e.g. map updating) and computer vision (e.g. target localization, automatic quality control), to name a few (Chen et al., 2007; Zitova and Flusser, 2003). Geo-registration is the process of registering an image with a map, or registering an image with another image that has been registered with a map, or finding the relationship between image coordinates (row, column) and ground coordinates (longitude, latitude) by means other than image registration (Li and Leung, 2004; Mao et al., 2001).

Coordinate transformations are required when it is necessary to register different sets of coordinates for objects in the same area that may have come from maps of different projections. In this case one or more sets of coordinates must be transformed so that they are represented in the same coordinate system as other sets.

*Corresponding author. E-mail: fkarsli@ktu.edu.tr. Tel: +90 462 3772769. Fax: +90 462 3250918.

After establishing the correspondence of the control points the mapping/transformation function is constructed by overlaying the sensed image on the reference one. The correspondence of the control points (CPs) from the sensed and reference images together with the fact that the corresponding CP pairs should be as close as possible after the sensed image transformation are employed in the mapping function design. The models of mapping functions can be divided into two broad categories according to the amount of supporting image data that is required. Global models use all CPs for estimating one set of mapping function parameters valid for the entire image. On the other hand, the local mapping functions treat the image as a composition of patches and the function parameters depend on the location of their support in the image. This leads to the tessellation of the image, usually a triangulation, of the parameters of the mapping function are separately defined for each patch (Brown, 1992).

The main objective of this paper is to describe a method of measuring the geometric distortion over the whole images instead of using a limited number of corresponding CPs coordinate differences. The method identifying the geometric deformations in entire digital images is proposed in this study. This method uses a test plate to measure the gray values in images which represent the geometric deformations in the image. The geometric deformations were determined using six geometric transformation and three resampling methods. For this purpose, a program was coded in Matlab software to register the image and detect the geometric deformation in the whole image based on pixel gray values. The experimental results are evaluated to discover the best transformation methods for image registration. The study comprises eight stages, from the image acquisition of the images to the evaluation of the images and subsequent results (Figure 1).

TRANSFORMATIONS FOR IMAGE REGISTRATION

This consists of a two stage process, the geometric transformation and the image resampling. The type and parameters of the mapping functions, aligning the sensed image with the reference image, are estimated in the first stage. The parameters of the mapping functions are computed by means of the established feature correspondence or control points. Then, the sensed image is transformed by means of the mapping functions. In the image resampling stage, the image values in non-integer coordinates are computed by the appropriate interpolation technique. In this study, six global mapping function and three interpolation methods were employed for digital image transformation to detect image deformation over the entire image area (Chen et al., 2007).

Geometric transformation

Geometric transformations are performed by mapping the pixel coordinates of the original image to another coordinate system to form a new image. They can perform the following operations on images: rotation, scaling, reflection and translation. Coordinate transformations are widely used in geodesy, surveying, photogrammetry and related professions. In photogrammetry they are used in the interior and exterior orientation of aerial photographs (Mikhail et al., 2001). In general, the effect of a transformation on a 2D or 3D object will vary from a simple change of location and orientation, with no change in shape or size, to a uniform change scale factor with no change in shape to changes of the shape and size of different degrees of nonlinearity (Mikhail, 1976; Andrei, 2006). The first geometric transformation method used for this study is non-reflective similarity transformation. It may include a rotation, a scaling and a translation. Shapes and angles are preserved. Parallel lines remain parallel and straight lines remain straight. Non-reflective similarity transformations are a subset of similarity transformations. It has four degrees of freedom and requires two pairs of points.

One of the most frequently used global models uses bivariate polynomials of low degrees. Similarity transform is the simplest model consisting of only rotation, translation and scaling. For a similarity, the equation is the same as for a non-reflective similarity. The mathematical model of similarity is as follows:

$$u = s(x\cos\varphi - y\sin\varphi) + t_x$$
$$v = s(x\sin\varphi + y\cos\varphi) + t_y \quad (1)$$

Where; s, φ and (t_x, t_y) are scaling, rotational and translational differences between the images, respectively (Tao and Hu, 2001). These parameters can be determined if the coordinates of two corresponding points in the images are known. This model is often called 'shape-preserving mapping' because it maintains angles and curvatures and is unambiguously determined by two CPs. Another linear model is an affine transform, which is slightly more general and

$$u = a_0 + a_1 x + a_2 y$$
$$v = b_0 + b_1 x + b_2 y \quad (2)$$

maps a parallelogram onto a square (Tao and Hu, 2001). This model is defined by three non-collinear CPs, preserves straight lines and the straight line parallelism. It can be used for multi-view registration assuming the following elements; the distance of the camera to the scene is large in comparison to the size of the scanned area, the camera is perfect (a pin-hole camera), the

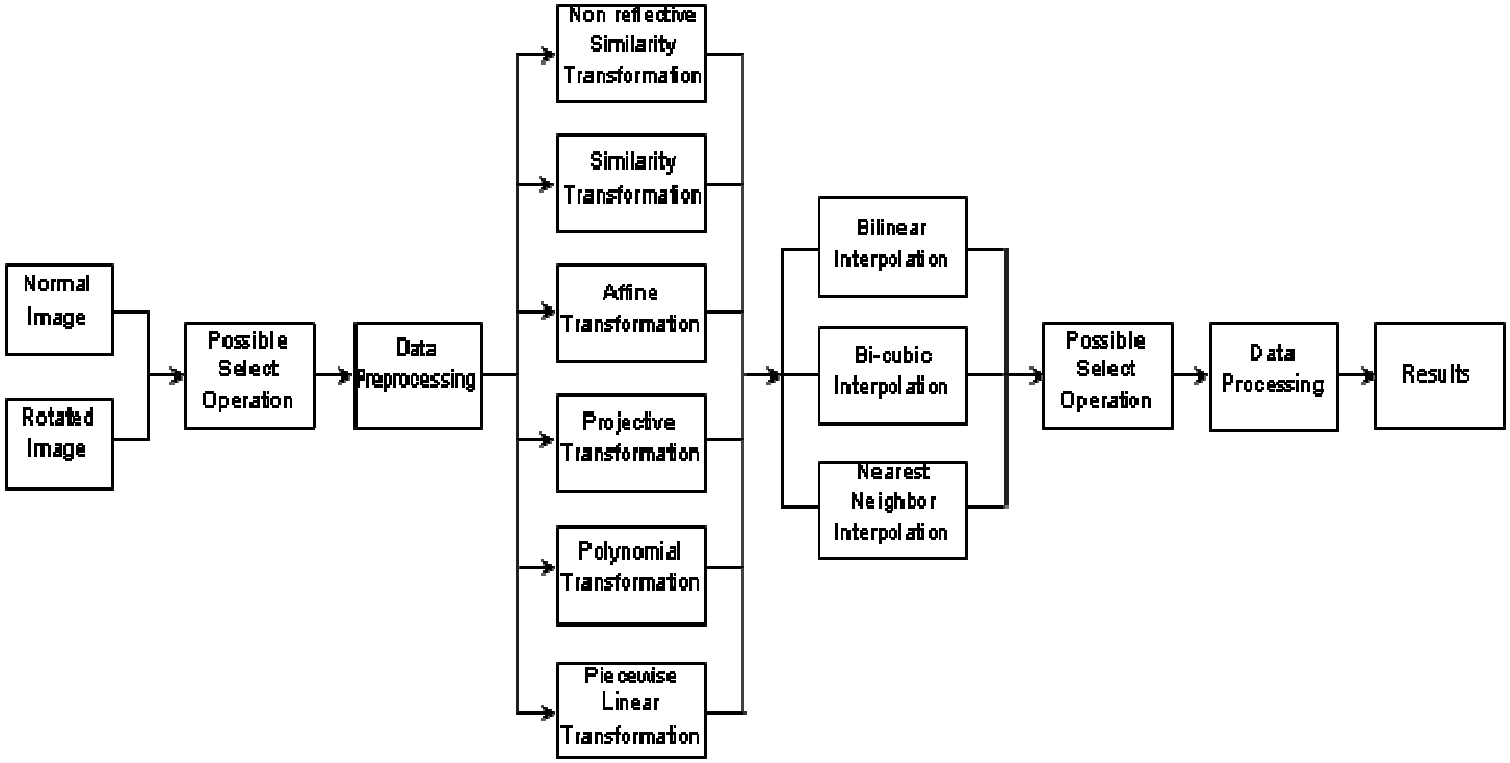

Figure 1. Workflow of the main parts of the study.

scene is flat and the present geometric distortion has no local factors. In an affine transformation, the *x* and *y* dimensions can be scaled or sheared independently and there may be a translation, a reflection, and/or a rotation. Similarities are a subset of affine transformations. For an affine transformation, the equation is the same as for a similarity and non-reflective similarity. This transformation supports non-isotropic scaling in addition to all the transformations that the non-reflective similarity transformation supports. It has six degrees of freedom that can be determined from three pairs of non-collinear points.

If the condition concerning the distance of the camera from the scene is not satisfied the following perspective projection model should be used (Novak, 1992);

$$u = \frac{a_0 + a_1 x + a_2 y}{1 + c_1 x + c_2 y}$$
$$v = \frac{b_0 + b_1 x + b_2 y}{1 + c_1 x + c_2 y} \quad (3)$$

This model is called projective transformation and it exactly describes a deformation of a flat scene photographed by a pin-hole camera the optical axis of which is not perpendicular to the scene. It can map a general quadrangle onto a square while preserving straight lines and it is determined by four independent CPs. Basically, a projective transformation is a transformation of an image that would be the same if the observer was not located in the same position but rather in the new coordinate system in which the image was transformed. Affine transformations are a subset of projective transformations. Projective transformation supports tilting in addition to all transformations that the affine transformation supports.

Another geometric transformation implemented for this study is the second or third order polynomial models (Lillesand and Kiefer, 2000). Higher order polynomials usually are not usually employed in practical applications because they may unnecessarily warp the sensed image in areas away from the CPs during the alignment with the reference image. In general, the number of CPs is usually higher than the minimum number required for the determination of the mapping function.

Polynomial transformations between two coordinate systems are typically applied in cases where one or both of the coordinate systems exhibit lack of homogeneity in orientation and scale. The small distortions are then approximated by polynomial functions in latitude and longitude. Depending on the degree of variability in the distortions, approximation may be carried out using 2nd, 3rd, or higher degree polynomials. In this study the 2nd degree polynomial was used. The form of a 2nd degree polynomial transformation (Tao and Hu, 2001) is:

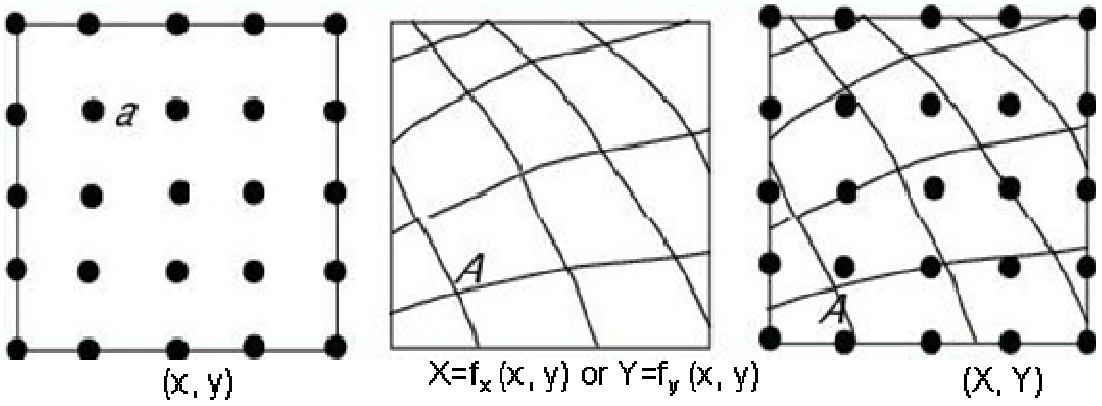

Figure 2. The resampling process a) Pixels in the reference image, b) A continuously sensed image, c) Overlaying the continuously and discretely sensed images.

$$x' = a_0 + a_1 x + a_2 y + a_3 x^2 + a_4 y^2 + a_5 xy + \cdots$$

$$y' = b_0 + b_1 x + b_2 y + b_3 x^2 + b_4 y^2 + b_5 xy + \cdots \quad (4)$$

The parameters of the mapping functions are then computed by means of the least-square fit, so that the polynomials minimize the sum of squared errors at the CPs. Such mapping functions do not exactly map the CPs onto their counterparts. This approach was proved to be very effective and accurate for satellite images (Zitova and Flusser, 2003).

The last geometric model used for this study is a piecewise linear transformation. In this transformation, affine transformations are applied separately to triangular regions of the image. If the control points in the reference image are triangulated, from the knowledge of the correspondence between the control points in the sensed and reference images, the corresponding triangles in the sensed image can be determined. Piecewise methods are those that map corresponding regions in the images to each other. If a linear transformation function is used to map a region in the sensed image to the corresponding region in the reference image, the transformation becomes piecewise linear. The transformation will be continuous but not smooth. When the regions are small or when the local geometric difference between the images is small, a piecewise linear method may produce satisfactory results. However, if local deformations are large, the gradients of the transformation on the two sides of a region boundary may be quite different, resulting in an inaccurate registration. Usually the triangles are used as regions in the piecewise linear method. In this example the triangular region in the upper-left part of the image remains unchanged while the triangular region in the lower-right part of the image is stretched (Goshtasby, 2005; McGlone, 1996).

Interpolation methods (Image resampling)

Having determined the mapping functions explicitly using of the control points, the next stage is to find points in the image corresponding to each location in the pixel grid previously defined over the image/map. The transformation;

$$X = f(x, y)$$
$$Y = g(x, y) \quad (5)$$

relates the coordinates of points in the reference image to the coordinates of the corresponding points in the sensed image. Given the (*x, y*) coordinates of a point in the reference image, the relationships given above (5) determine the (*X, Y*) coordinates of the corresponding point in the sensed image. By reading the intensity at (*X, Y*) in the sensed image and saving at (*x, y*) in a new image, the sensed image is point-by-point resampled to the geometry of the reference image. Therefore, to resample the sensed image, the reference image is scanned and, for each pixel location, the corresponding location is determined in the sensed image. Although (*x, y*) are integers, (*X, Y*) are floating-point numbers. Since intensities at only integer coordinates are available in the sensed image, the intensity at point (*X, Y*) has to be estimated from the intensities of a small number of surrounding. Figure 2 depicts the resampling process. Pixel *a* in the reference image puts on to point *A* in the continuous sensed image. To estimate the intensity at *A*, intensities in a small neighborhood of *A* in the discrete sensed image are used. Different methods to achieve this estimation have been developed. In the following sections, the nearest-neighbor, bilinear interpolation, cubic convo-lution, cubic spline interpolation and radially symmetric resampling methods are discussed. However, only the first three resampling methods were utilized for

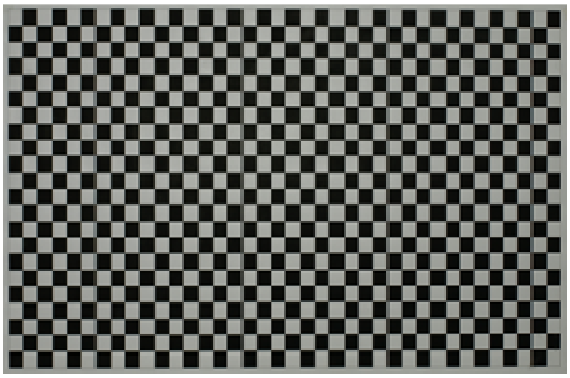

Figure 3. Test plate used for image registration.

this study.

Several survey papers on resampling techniques have been published in the last few years. A detailed investigation and comparison of methods was carried out by Parker and Kenyon (1983) for 2D images and by Grevera and Udupa (1998) for 3D data. Thevenaz and Blu (2003) paid attention to the elimination of undesired interpolation artifacts. Lehmann et al. (1999) published a survey article covering main interpolation methods with the emphasis on medical imaging applications. There are three common methods for resampling: nearest neighbour, bilinear interpolation and cubic convolution (Zitova and Flusser, 2003).

Nearest neighbour

This resampling uses the digital value from the pixel in the original image that is the nearest to the new pixel location in the corrected image. This is the simplest method and does not alter the original values, but may result in some pixel values being duplicated while others are lost. This method also tends to result in a disjointed or blocky image appearance.

Bilinear interpolation

This resampling takes a weighted average of four neighbouring pixels in the original image to the new pixel location. The averaging process alters the original pixel values and creates entirely new digital values in the output image. This may be undesirable if further processing and analysis, such as classification based on spectral response, is to be done. If this is the case, resampling may best be carried out after the classification process.

Cubic convolution

This resampling goes even further by calculating a distance weighted average of a block of sixteen pixels from the original image that surround the new output pixel location. As with bilinear interpolation, this method results in completely new pixel values. Both these methods produce images that are much sharper appearance and avoid the blocky appearance of the nearest neighbour method (Goshtasby, 2005).

MATERIALS AND METHODS

In the first stage image data was acquired. This is the process of converting a picture into its numerical representation, which is suitable for the image registration stages. In order to achieve the best results, it is important to start with good-quality digital images of the test plate. An Olympus E510 digital SLR camera was used for the study. It contains a 10.9 megapixel CCD sensor (3648 × 2736 pixel with approximately 5 µm pixel spacing) with a format size of 18.25 × 13.7 mm. The camera system has two different lenses (14 - 42 mm and 40 - 150 mm). To register the image this study used a planar test field (Figure 3), which is a plate with a regular grid. It has 38 × 22 black and white grids each cell measuring 18 × 14 mm. Some of the grid corners were used as control points. To correct the geometry of rotated image, the test plate was placed in front of the camera and images were obtained. The illumination of the scene and the shutter speed of the camera were varied during the acquisition of the images. Two images with 3648 × 2736 pixel resolution were taken for a 42 mm focal lenght setting from a distances 1.5 m. One of them was taken with a normal position, the other was taken at 30 - 35 degrees by rotating the camera. These two images were then used as the inputs.

In this study, proposed method used radiometric pixel gray values in images to represent the geometric deformations over the entire image surface, measuring test plate. Geometric transformation and resampling methods were applied to a rotated image for registering it on normal image using an in-house program designed in this study. The program uses control points to register the images if projective, polynomial and piecewise linear transformations are to be used. The control points cannot be used for the other geometric methods, instead, the scale and rotation angle between normal and rotated images should be provided for these methods. Nine corrresponding control points were selected from both the normal and rotated image to determine the geometric deformations. The selection process of corresponding control points in the program is shown in Figure 4. These points are regularly distributed on image. It should be mentioned that using a larger number of grid points may not necessarily improve the geometry correction accuracy. Using 12 points, errors were obtained that were similar to those obtained using nine points. Correspondingly, if deformation across an image varies smoothly, a few point correspondences are sufficient to satisfactorily correct the geometry of the image.

The image registration for the rotated image was implemented by defining the transformation function with corresponding control points. After correcting the geometry of the rotated image, three color bands (red, green, blue) of the normal and corrected image were extracted from each other in order to distinguish distortions in entire image. In this stage, the corresponding gray values of the two images are mathematically subtracted. In fact, the new image constitutes of the gray value differences for each band. This is called as “error surface” or “subtracted image” (Figure 5a). The average and standard deviation of gray value differences for the three color bands were computed for each combination of geometric and resampling method. Histogram graphics of subtracted images were drawn for each color bands. It can be seen from the histogram graphics that the gray level differences are close to zero. Highest frequency value in histogram shows that the parts where the largest geometric error densifies in whole image. As a result of this, methods have been compared to find the best method.

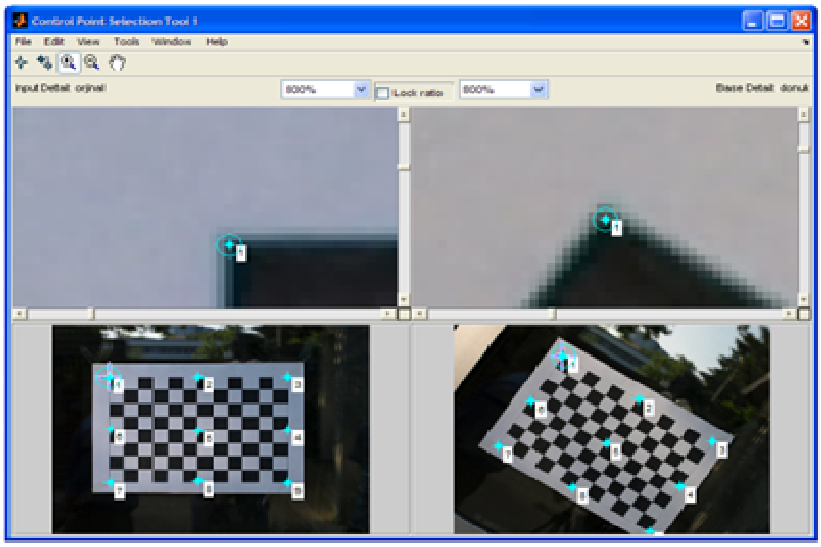

Figure 4. Selection of control points and their distribution on images using the program designed for the study.

(a)

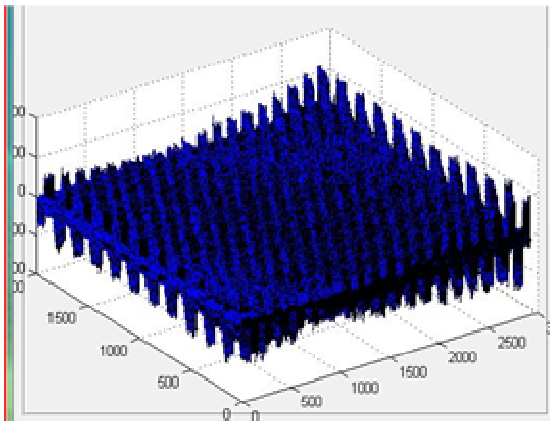

(b)

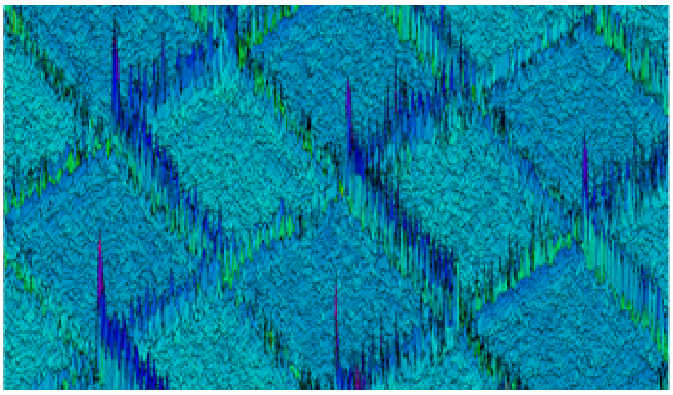

Figure 5. Results for similarity transformation and nearest neighbor methods; a) error surface, b) enlarged view of error surface for red band.

Furthermore, the geometric distortions were also calculated using the corresponding grid corners of pixel coordinates between the normal and registered images. Then, the coordinate differences of grid corners were obtained and represented as a vector structure on the image. From this the location of the maximum error vector in the image can be detected. According to the results obtained, the best geometric and resampling method combination was determined, the details are given below.

RESULTS AND DISCUSSION

One of the problems frequently encountered in application of photogrammetry and remote sensing is the accuracy of the geometric and radiometric transformation. Accuracy analysis was provided in past studies and accuracy of control points was tested in those studies (Goshtasby, 1988; Novak, 1992; Zhang, 2007). Hovewer, it is obvious that the most accurate detection of image deformation is based on pixel analysis. From the results of the combination with the geometric and resampling method for each pixel, examining the radiometric values, it can be obtained that the the results giving information about accuracy of transformation and resampling method based on pixel. In this study, in order to evaluate the effectiveness of the geometric deformation methods, the test plate shown in Figure 3 was used.

In order to model geometrical errors on images covering test area, the result images were generated using a combination of six geometric and three resampling methods. As mentioned in the previous section, the resulting images were subtracted images or error surface images. As seen in Figure 4, for all methods 9 control points were choosen on the corner, edge central part and central part of the image. Thus all control points were uniformly distributed over the test area.

When the results are examined in detail for the red bands for all the methods, it can be seen that the gray values differ from each other between neighbouring pixels groups and in particular, the error magnitudes are slightly increased at the grid transitions or corners. This results from the geometric and radiometric transformations.

Firstly, similarity transformation and nearest neighbour methods were applied to the image of test plate, then errors were sketched like a vector for each pixel location and surface of these vectors was created (Figure 5a). On this surface, the directions of the vectors computed by extracting the images were also depicted. The images used for this process were normal and rotated. In Figure 5, when general error surface was examined for this method, errors were distributed over the image surface and they were mainly towards negative direction. The errors computed with similarity and nearest neighbour methods for red band were also shown by zooming in Figure 5b.

All combinations of geometric and radiometric methods were applied to the test plate images and their color bands to generate the error surfaces. Similarity transformation and non-reflective similarity transformation with the combination of all resampling methods was carried out on all color bands and the results that were obtained are shown as histogram in Figure 6. The histogram graphics show the gray values differences frequency for all color bands of selected images. The average errors for the different methods are also given in Table 1. Enlarged vector results have been showed for selected sample part of the red band in Figure 5b.

For affine transformation and nearest neighbour method, the same process was implemented by applying these methods to test image. Then, residual errors were drawn as a vector for each pixel and the surface was created (Figure 7a). On this surface the direction of computed residuals were seen. From Figure 7a, it has been seen that residual errors have become dense at edge pixels. Figure 7b shows the magnified view of the error vectors computed with affine and nearest neighbour methods for the red band.

The combination of the affine transformation and all the resampling methods tested in all color bands and acquired results are shown in Figure 8. These histograms show the frequency of gray scale differences according to the selected combinations such as affine and nearest neighbour. The average error magnitudes related to this method are also given in Table 1.

Figure 9a shows the results of the projective transformation and nearest neighbour method performed on the image of the test plate. The error magnitudes were drawn as a vector for each pixel position and surface of these errors was generated. On this surface direction of errors can be seen. From Figure 9a, when the general error surface is examined from the distribution of the error values on the image surface it can be seen that they are mainly towards negative direction. Figure 9b shows an enlarged view of a part of error surface for the red band acquired using the projective transformation and nearest neighbour methods.

Projective transformation with a combination of all resampling methods has been examined for all color bands and the results obtained are shown in Figure 10 as histograms. Also the average errors related to this method are given in Table 1. In Figure 9b the detailed results are shown for a selected sample part on the red band.

Figure 11a represents that polynomial transformation and nearest neighbour method has been implemented for the test plate image. The error magnitudes are sketched as a vector for each pixel position and its surface is created. The direction of the computed errors can also be seen on this surface. When the general error surface was surveyed using the method in this figure, the errors was distributed from the central point to the edge pixels of the image.This distribution decreases from central image to the edge pixels. An enlarged part of the error surface can be seen in Figure 11b. A combination of all the resampling methods with polynomial transformation was

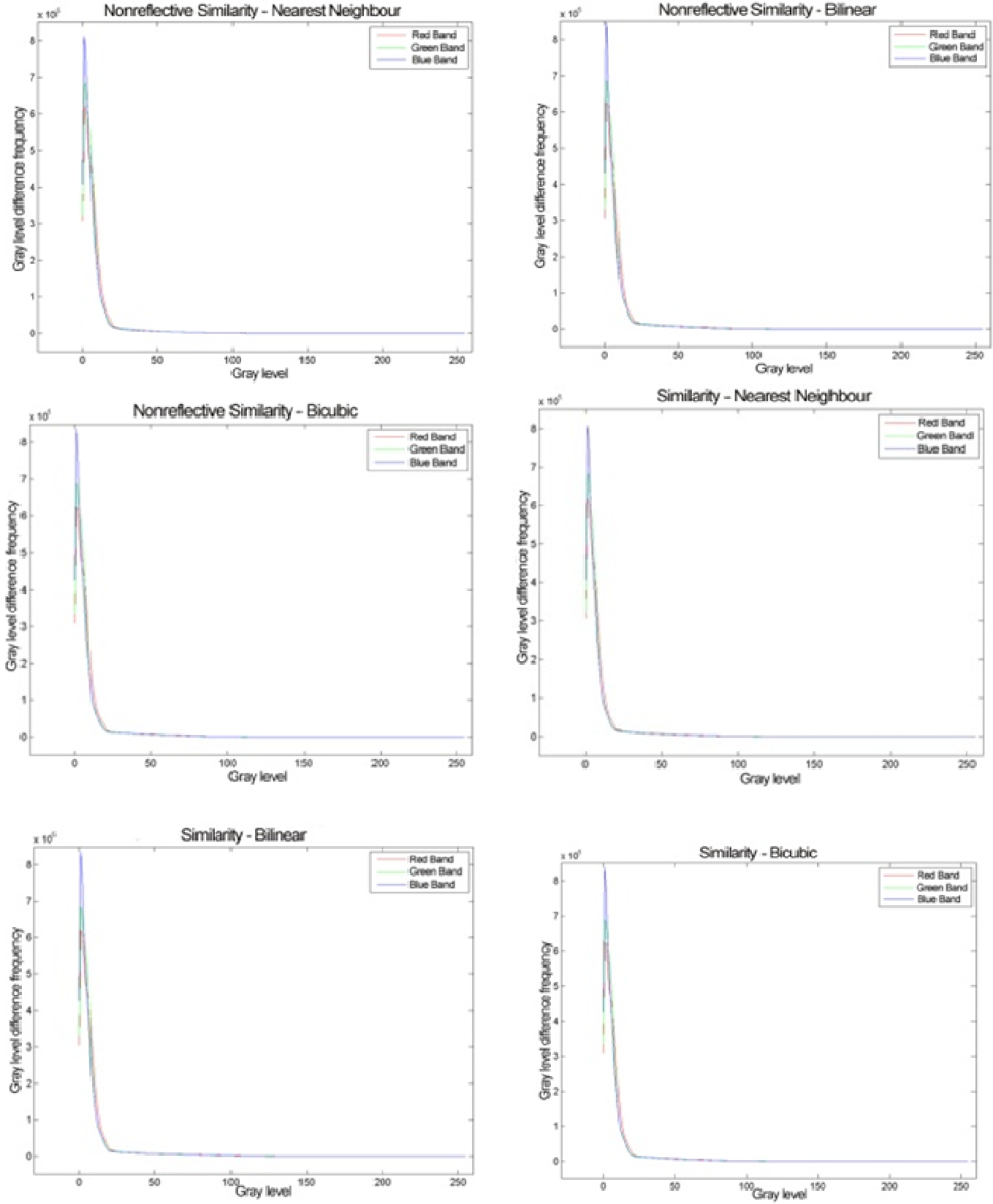

Figure 6. Errors and gray value histogram graphics for similarity and non-reflective similarity methods.

Table 1. Gray value differences and standard deviations using geometric and radiometric methods.

Geometric transformation method	Resampling method	Red band		Green band		Blue band	
		Mean	Standard deviation	Mean	Standard deviation	Mean	Standard deviation
Similarity	Nearest neighbour	8.86	13.13	8.21	12.91	7.78	12.68
	Bilinear	9.94	16.31	9.23	15.85	8.71	15.48
	Bicubic	8.69	12.77	8.02	12.55	7.58	12.31
Non-reflective similarity	Nearest neighbour	8.28	11.55	7.72	11.58	7.40	11.69
	Bilinear	8.73	12.75	8.09	12.54	7.60	12.31
	Bicubic	8.69	12.77	8.02	12.55	7.58	12.31
Affine	Nearest neighbour	8.90	13.60	8.28	13.58	7.73	13.09
	Bilinear	9.94	16.31	9.23	15.85	8.71	15.48
	Bicubic	8.69	12.77	8.02	12.55	7.57	12.31
Projective	Nearest neighbour	10.71	18.41	10.17	18.58	9.90	18.73
	Bilinear	12.27	22.23	11.68	22.24	11.37	22.27
	Bicubic	10.59	18.22	10.04	18.41	9.75	18.56
Polynomial	Nearest neighbour	10.88	18.78	10.36	18.96	10.12	19.21
	Bilinear	10.74	18.42	10.23	18.61	9.95	18.87
	Bicubic	10.77	18.58	10.23	18.77	9.99	19.04
Piecewise linear	Nearest neighbour	10.44	17.34	9.92	17.28	9.89	18.13
	Bilinear	10.31	17.00	9.81	16.95	9.75	17.81
	Bicubic	10.31	17.12	9.78	17.07	9.76	17.93

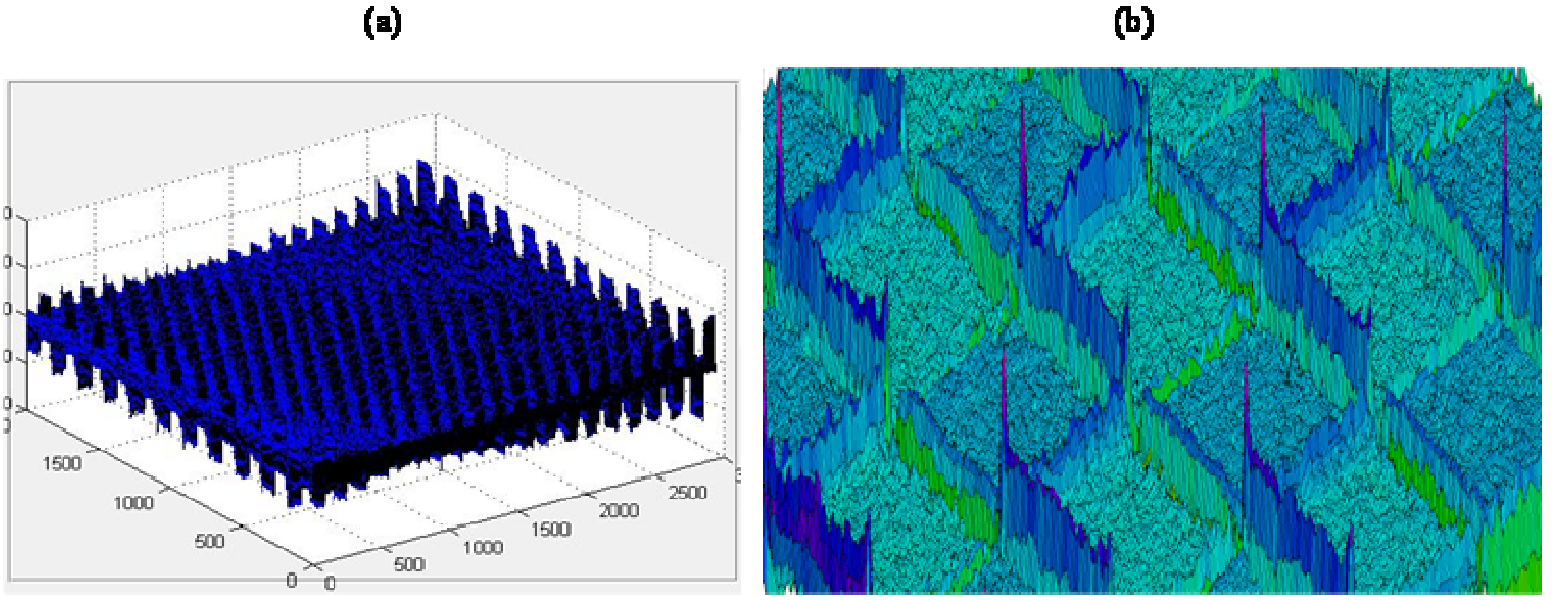

Figure 7. Affine transformation and nearest neighbor methods results; a) error surface, b) enlarged view of error surface for red band.

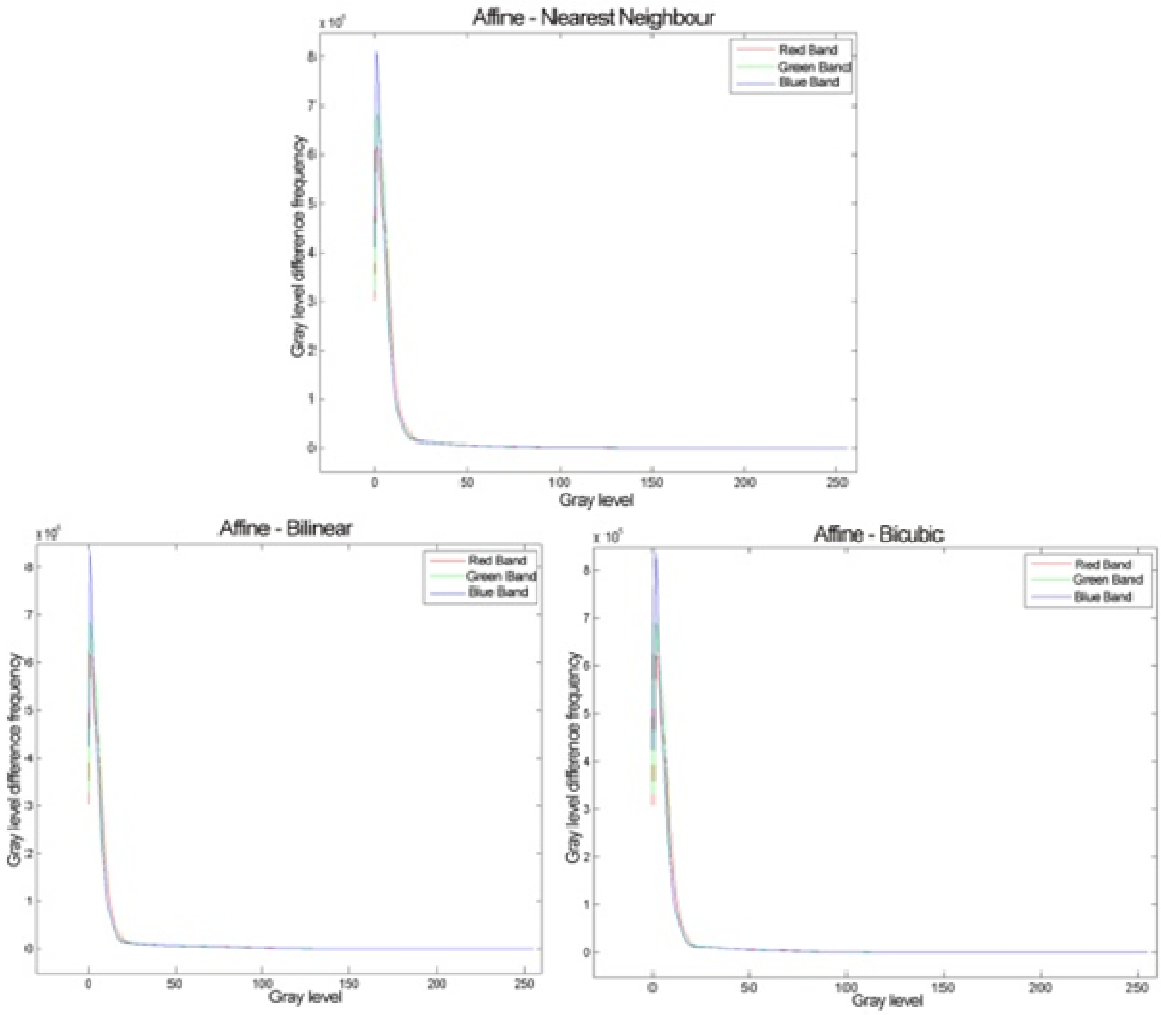

Figure 8. Errors and gray value histogram for affine methods.

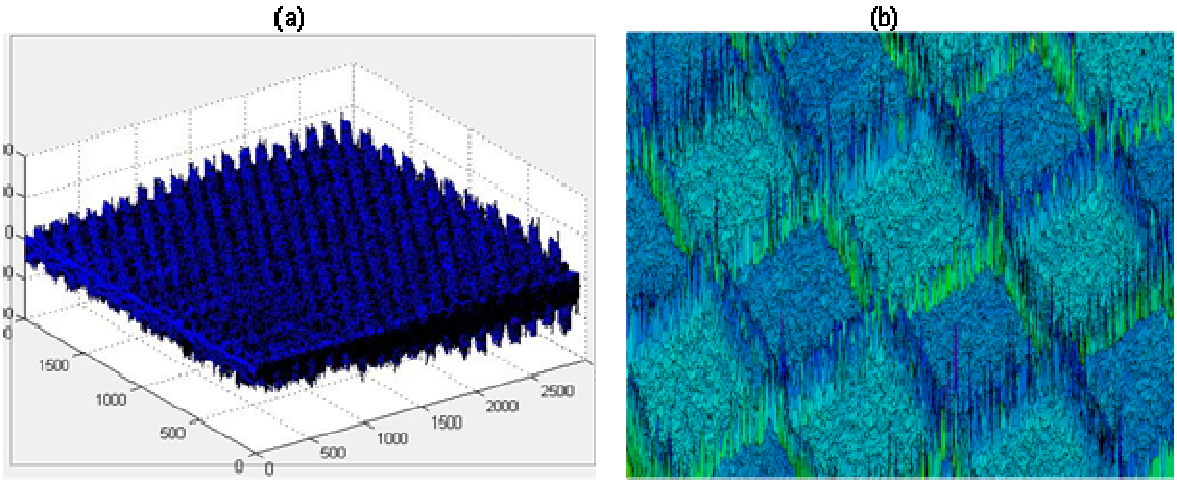

Figure 9. Results for projective transformation and nearest neighbor methods; a) error surface, b) enlarged view of error surface for red band.

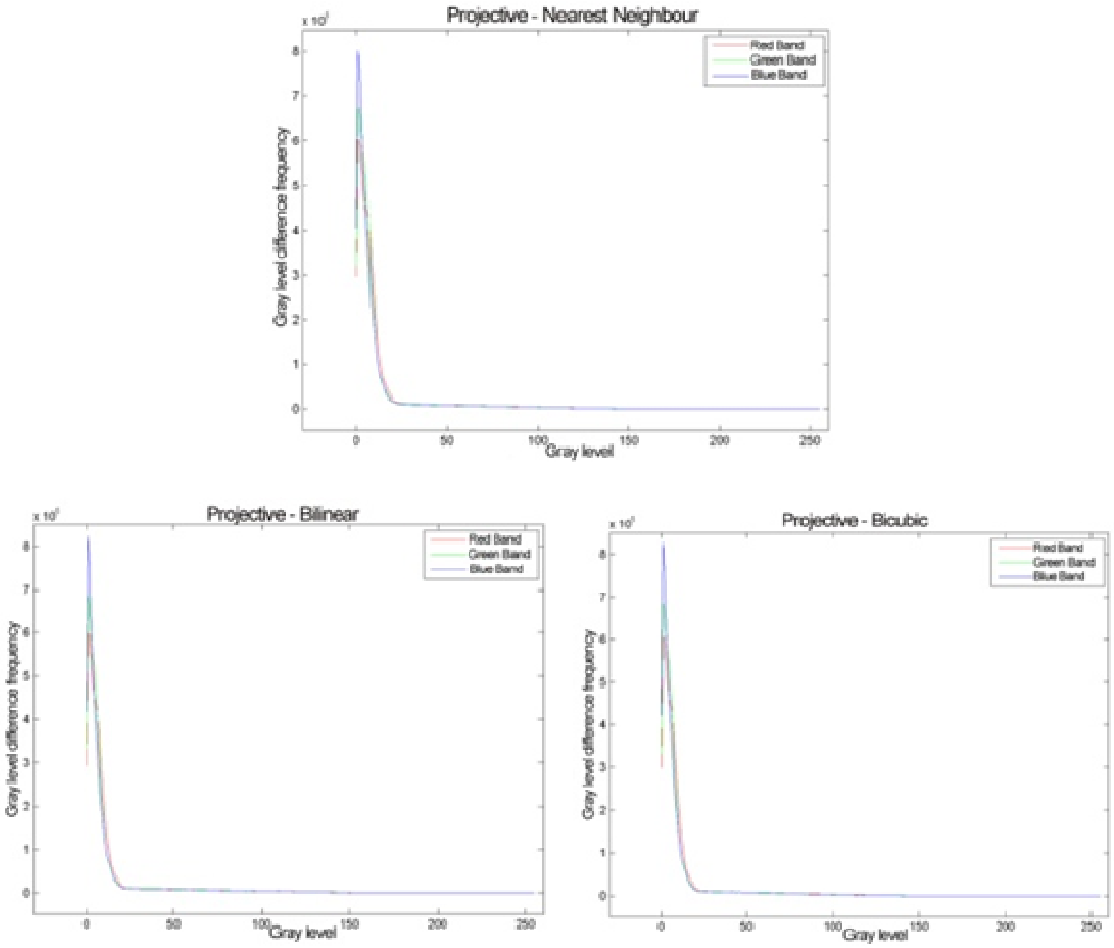

Figure 10. Errors and gray values for projective methods.

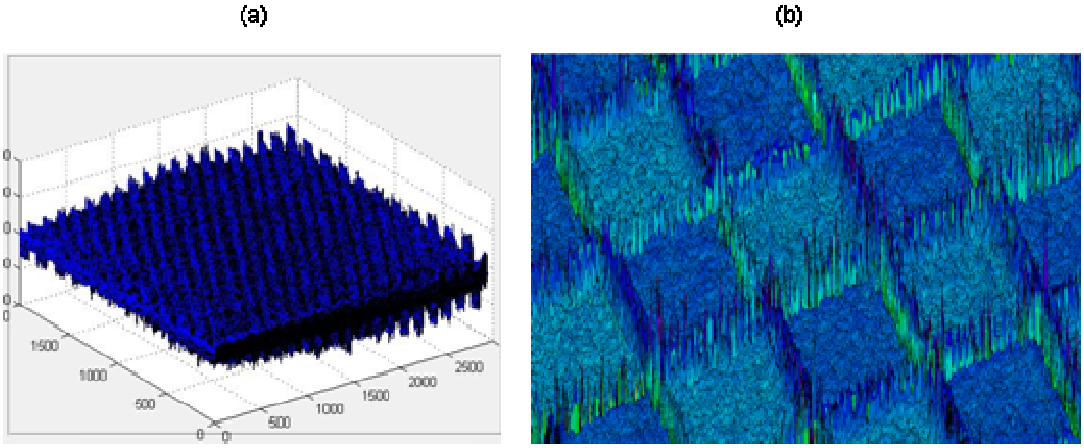

Figure 11. Results for polynomial transformation and nearest neighbor methods; a) error surface, b) enlarged view of error surface for red band.

tested for all color bands and the results obtained are shown in Figure 12. The average errors related to this method are given in Table 1. In Figure 11b, detailed results are shown for selected sample section of the red band.

In Figure 13a, the piecewise linear transformation and

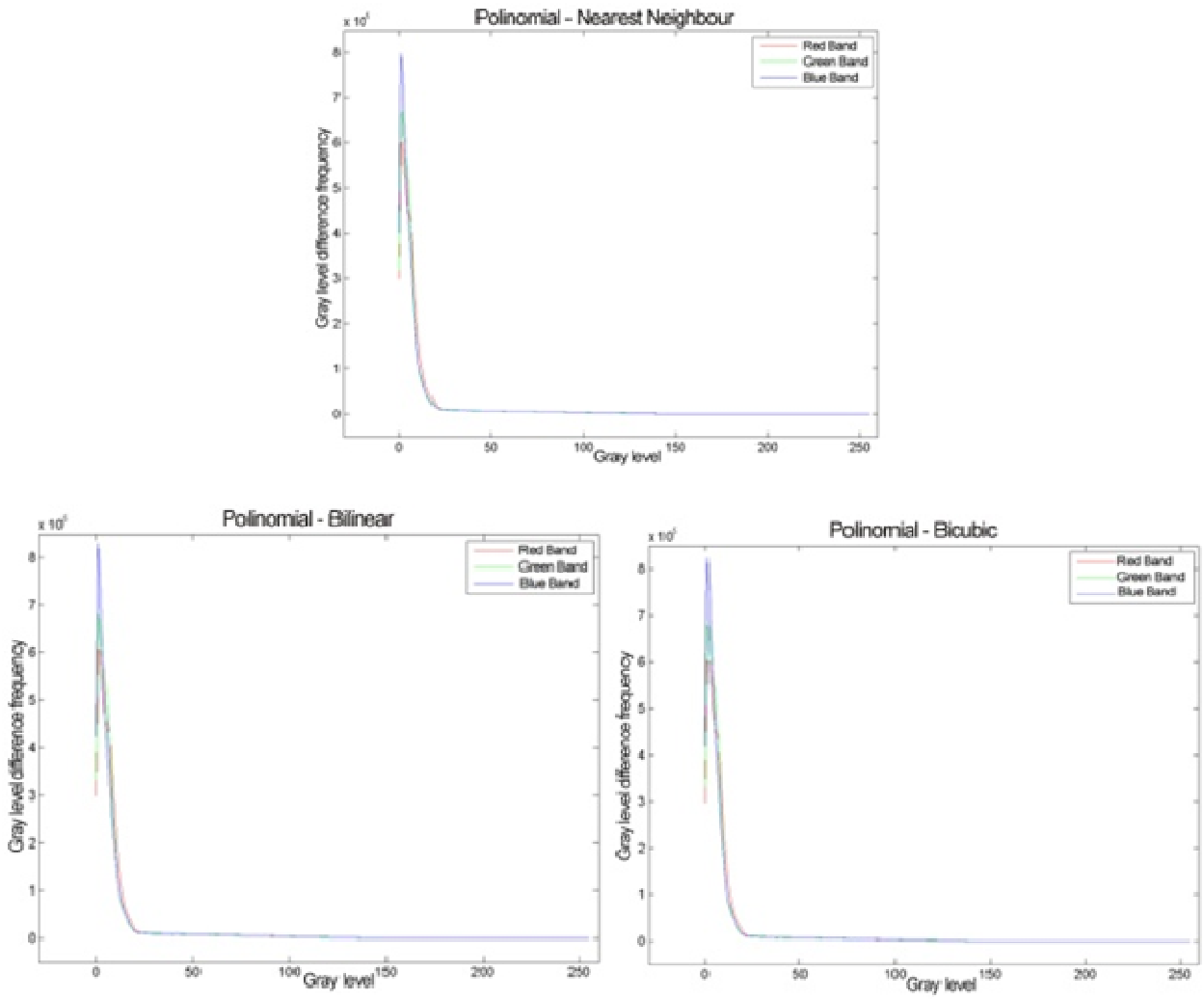

Figure 12. Errors and gray value histogram for polynomial methods.

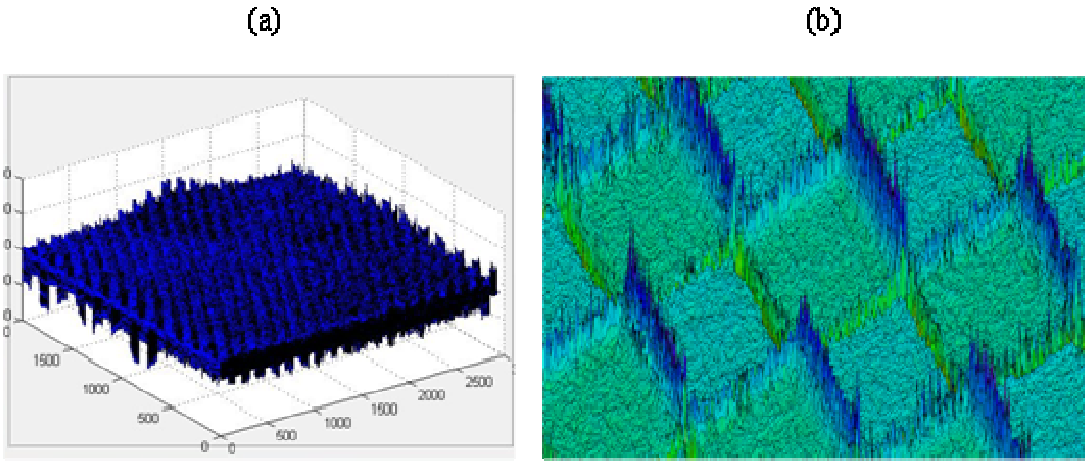

Figure 13. Piecewise linear transformation and nearest neighbour methods results; a) error surface, b) enlarged view of error surface for red band.

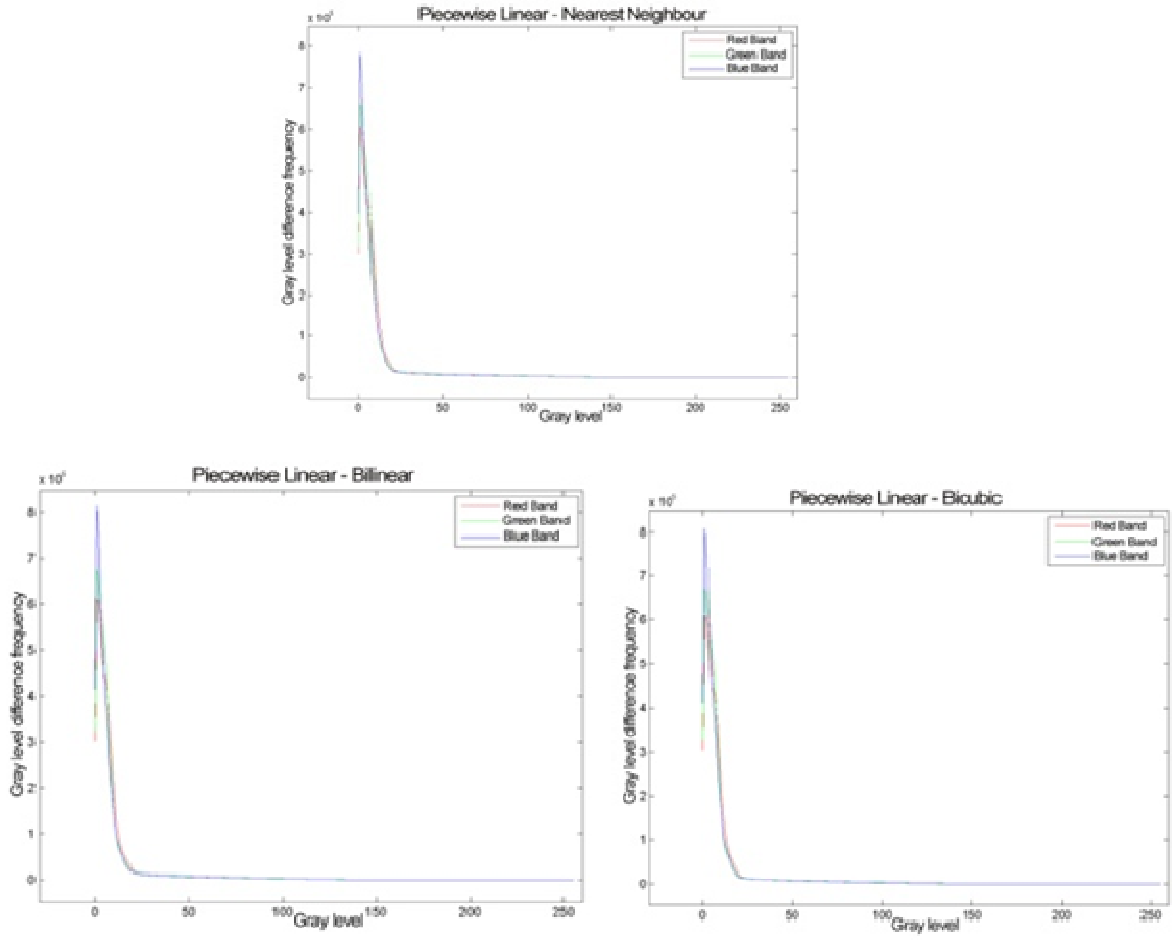

Figure 14. Errors and gray values for piecewise linear transformation methods.

nearest neighbour method were carried out on the image of the test plate. The error magnitudes were drawn as a vector for each pixel location and its surface was constructed, on this surface direction of the computed error was shown. Figure 13a shows the results of the examination of the general error surface, with the errors being distributed dependent on the effect of the computation algorithm. Figure 13b shows the enlarged view of the red band error vectors computed by the application of piecewise linear transformation nearest neighbour method.

The piecewise linear transformation with the combination of all resampling methods was applied to all color bands and the results gained are shown in Figure 14 as histogram graphics. As in previous applications, the average errors related to this method are given in Table 1. The detailed results are shown in Figure 13b for selected sample section of the red band.

When Table 1 was analyzed, it was found that geometric transformations and resampling methods were implemented on three bands of image. From Table 1 when similarity transformation results were examined, nearly on all color bands gray value differences are equal, but for the bilinear resampling with this method was employed error increased on a small scale. In the same table for non-reflective similarity transformation, the averages of the blue band were smaller than the other bands and when nearest neighbour resampling method was applied the error values are smaller than those of the other resampling methods. In Table 1 for affine transformation when nearest neighbour and bicubic resampling methods were applied, the average of gray values were equal to each other as it was in non-reflective transformation, but the errors increased due to the bilinear method average values. For the projective transformations, the averages of the gray value distinctions were greater than those obtained in the other transformations. The averages of the gray value differences were equal to nearest neighbour and bicubic resampling methods; however, in the bilinear resampling method the average was greater than the other methods. Once again from Table 1 when polynomial transformation was examined, the averages of all the band differences were equal, but the errors were slightly higher using nearest neighbour resampling method. Finally, for the piecewise linear transformation, the averages of all band differences were

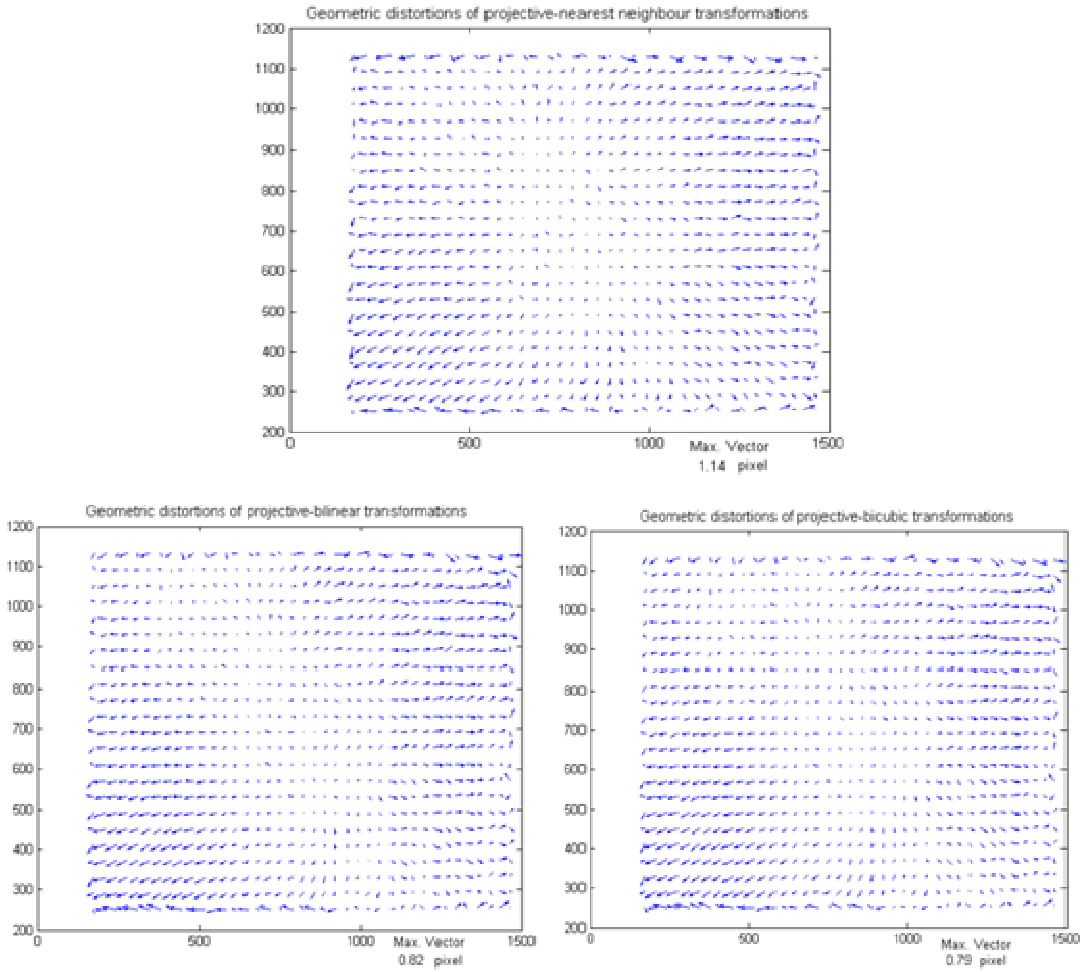

Figure 15. Maximum geometric differences between the grids on the normal and corrected images for projective transformation with all resampling methods

equal and the errors increase when using the nearest neighbour resampling method as in polynomial transformation. As shown in Table 1 generally, the average of the gray value differences for the non-reflective similarity, similarity and affine transformations were equal. Furthrmore, the differencies of the gray value averages computed for projective, polynomial and partial linear transformations were equal and greater than the other three methods.

In this study, the geometrical distortions over the whole image were also determined by calculating the geometric vectors between the grid points in the normal image and rotated/corrected image. This process was implemented selecting different geometric and resampling method combinations. Maximum vector was determined as 2.75 pixels with the similarity and nearest neighbour combination. As seen in Table 2, the best and minimum results were obtained using projective transformation with all the resampling methods. All the combinations of the methods gave the same results for the average. Hovewer, the results can be divided two groups; the first, three methods gave equal values to the vectors in terms of geometric errors. The remainder has the same quality for geometric errors. The projective transformation produced the best results (Table 2). The geometric errors calculated by this method for the image sapce are illustrated in Figure 15 where it can be seen that the vector values extend maximum magnitudes towards the image corner.

Conclusions

In this paper, a new method covering six geometric and three radiometric transformation techniques were investigated for image registration. An overview of the theoretical background and methodologies in image transformation using digital photogrammetry, remote sensing and sensing and other disciplines were presented.

Table 2. Maximum geometric differences between the grids on normal and corrected images.

Transformation method	Resampling method (Maximum vector value)		
	Nearest neighbour	Bilinear interpolation	Cubic convolution
Non-reflective Similarity	2.69	1.96	2.02
Similarity	2.75	1.96	2.02
Affine	2.69	1.96	2.02
Piecewise Linear	1.53	1.51	1.52
Projective	1.14	0.82	0.79
Polynomial	1.54	1.04	1.02

Rather than modelling the geometric distortions with control points extracted by using different geometric transformation and resampling methods, geometric distortions were determined over the whole digital image by using gray level differences for image registration. Experimental results of the all methods on images acquired were presented and evaluated.

This study has proved that the geometric distortions both come from geometric transformation and resampling method can be determined all over the image surface. The locations of the errors on the images are more important rather than their magnitude. When methods were compared it was observed that the largest digital values related the gray value differences were directly affected by the accuracy of geometric and resampling method and the selection test area on the image. This issue can be regarded as negative part of this study.

According to the results produced in this study, non-reflective similarity, similarity and affine transformation give better accuracy than other methods. This shows their robustness compared to the others. With reference to the grid corners of coordinate differences, the projective transformation method combined with all the resampling techniques produced the best results.

In conclusion, the results of the experiments show that this new pixel based method can be used successfully for image registration. It can also be used to detect geometric deformation in the entire image using gray value differences in the pixel level.

REFERENCES

Andrei CO (2006). 3D affine coordinate transformations. MSc in Geodesy, School of Architecture and the Built Environment, Royal Institute of Technology (KTH), Stockholm, Sweden.

Brown LG (1992). A Survey of image registration techniques. ACM Comp. Surv. 24(4): 325-376.

Chen FC, Chen MH, Li HT (2007). Fully Automatic and Robust Approach for Remote Sensing Image Registration. In Rueda et al. (eds) CIARP 2007, LNCS: Springer-Verlag Berlin Heidelberg 4756: 891-900.

Goshtasby AA (1988). Registration of images with geometric distortions. IEEE Trans. Geosci. Remote Sensing 26: 60-64.

Goshtasby AA (2005). 2-D and 3-D Image Registration. John Wiley & Sons, Inc, ISBN 0-471-64954-6.

Grevera GJ, Udupa JK (1998). An objective comparison of 3D image interpolation methods. IEEE Trans. Med. Imaging 17: 642-652.

Lehmann TM, Gonner C, Spitzer K (1999). Survey: interpolation methods in medical image processing, IEEE Trans. Med. Imaging 18: 1049-1075.

Li W, Leung H (2004). A Maximum Likelihood Approach for Image Registration Using Control Point And Intensity. IEEE Trans. Image Process. 13(8): 1115-1127.

Lillesand TM, Kiefer RW (2000). Remote Sensing and Image Analysis, 4th Edition,John Wiley and Sons, New York. p. 736.

Mao Z, Pan D, Huang H, Huang W (2001). Automatic registration of SeaWiFS and AVHRR imagery. Int. J. Remote Sensing 22(9): 1725-1735.

McGlone C (1996). Sensor modeling in image registration, In Greve CW (eds.), Digital Photogrammetry: An Addendum, ASPRS, pp. 115-123.

Mikhail EM (1976). Observations and Least Squares. New York, New York: IEP/A.Dun-Donelley.

Mikhail EM, Bethel JS, McGlone JC (2001). Introduction to Modern Photogrammetry, John Wiley and Sons, Inc., New York.

Novak K (1992). Rectification of digital imagery, Photogrammetric Eng. Remote Sensing 58(3): 339-344.

Parker JA, Kenyon RV, Troxel DE (1983). Comparison of interpolating methods for image resampling. IEEE Trans. Med. Imaging 2: 31-39.

Tao CV, Hu Y (2001). Use of the rational function model for image rectification. Canadian J. Remote Sensing 27(6): 593-602.

Thevenaz P, Blu T, Unser M (2003). Image interpolation and resampling, Handbook of Medical Image Processing, Academic Press, New York.

Zhang C, Fraser CS (2007). Automated registration of high-resolution satellite images, The Photogrammetric Record, 22(117): 75-87.

Zitova B, Flusser J (2003). Image registration methods: Survey Image Vision Comput. 21: 977-1000.